




Article

Reduced Graphene-Oxide-Encapsulated MoS₂/Carbon Nanofiber Composite Electrode for High-Performance Na-Ion Batteries

Su-Ho Cho ^{1,†} , Jong-Heon Kim ^{2,†}, Il-Gyu Kim ³, Jeong-Ho Park ³, Ji-Won Jung ^{3,*}, Hyun-Suk Kim ^{2,*} and Il-Doo Kim ^{1,*}

¹ Department of Materials Science and Engineering, Korea Advanced Institute of Science and Technology (KAIST), Daejeon 34141, Korea; caca1108@kaist.ac.kr

² Department of Materials Science and Engineering, Chungnam National University, Daejeon 34134, Korea; mapig2@naver.com

³ School of Materials Science and Engineering, University of Ulsan, Ulsan 44776, Korea; ilgyu.kim.96@gmail.com (I.-G.K.); fjdk9936@naver.com (J.-H.P.)

* Correspondence: jwjung4@ulsan.ac.kr (J.-W.J.); khs3297@cnu.ac.kr (H.-S.K.); idkim@kaist.ac.kr (I.-D.K.)

† S.-H.C. and J.-H.K. contributed equally to this work.

Abstract: Sodium-ion batteries (SIBs) have been increasingly studied due to sodium (Na) being an inexpensive ionic resource (Na) and their battery chemistry being similar to that of current lithium-ion batteries (LIBs). However, SIBs have faced substantial challenges in developing high-performance anode materials that can reversibly store Na⁺ in the host structure. To address these challenges, molybdenum sulfide (MoS₂)-based active materials have been considered as promising anodes, owing to the two-dimensional layered structure of MoS₂ for stably (de)inserting Na⁺. Nevertheless, intrinsic issues of MoS₂—such as low electronic conductivity and the loss of active S elements after a conversion reaction—have limited the viability of MoS₂ in practical SIBs. Here, we report MoS₂ embedded in carbon nanofibers encapsulated with a reduced graphene oxide (MoS₂@CNFs@rGO) composite for SIB anodes. The MoS₂@CNFs@rGO delivered a high capacity of 345.8 mAh g⁻¹ at a current density of 100 mA g⁻¹ for 90 cycles. The CNFs and rGO were synergistically taken into account for providing rapid pathways for electrons and preventing the dissolution of S sources during repetitive conversion reactions. This work offers a new point of view to realize MoS₂-based anode materials in practical SIBs.

Keywords: molybdenum sulfides; carbon nanofibers; reduced graphene oxides; anodes; sodium-ion batteries



Citation: Cho, S.-H.; Kim, J.-H.; Kim, I.-G.; Park, J.-H.; Jung, J.-W.; Kim, H.-S.; Kim, I.-D. Reduced Graphene-Oxide-Encapsulated MoS₂/Carbon Nanofiber Composite Electrode for High-Performance Na-Ion Batteries. *Nanomaterials* **2021**, *11*, 2691. <https://doi.org/10.3390/nano11102691>

Academic Editor: Carlos Miguel Costa

Received: 15 September 2021

Accepted: 11 October 2021

Published: 13 October 2021

Publisher's Note: MDPI stays neutral with regard to jurisdictional claims in published maps and institutional affiliations.



Copyright: © 2021 by the authors. Licensee MDPI, Basel, Switzerland. This article is an open access article distributed under the terms and conditions of the Creative Commons Attribution (CC BY) license (<https://creativecommons.org/licenses/by/4.0/>).

1. Introduction

A battery of things (BoT)—first mentioned by Tony Seba, the author of “Clean Disruption of Energy and Transportation”—has come for modern society, requiring battery-powered devices everywhere [1]. Current lithium-ion batteries (LIBs), with a high energy density of ~250 Wh kg⁻¹, have been considered to be promising energy storage systems combined with renewable energy technologies [2]. Despite the viability of LIBs, utilization of the state-of-the-art LIBs for an energy storage system (ESS) has been restricted due to finite reserves of Li⁺ on earth, which would increase the price of Li sources used for large-scale applications [3]. Among alternatives to LIBs, sodium-ion batteries (SIBs) with a similar battery chemistry (redox potential of −2.71 V vs. SHE) as LIBs have constituted an exciting avenue for advancing ESSs [4,5].

However, anode materials with low energy density have impeded the development of SIB technologies. To address this issue, many promising candidates (e.g., hard carbon, metal oxides/sulfides/selenides, etc.) with high capacities have been suggested so far [6–12]. However, carbonaceous materials show limited use due to their low specific capacity and

less reversible capacity, and transition metal oxides (TMOs) need to be changed due to their low conductivity. As high-capacity anodes, sulfide-based materials such as FeS₂ and Sn₂S have been developed because transition metal sulfides (TMSs) have a higher electronic conductivity as well as an excellent ability to store Na⁺ [11,12]. Among them, molybdenum sulfide (MoS₂)-based anode materials possessing large interlayer spaces (0.615 nm) between two-dimensional (2D) MoS₂ slabs could allow facile (de)insertion of Na⁺ with few structural changes during conversion reactions ($\text{MoS}_2 + 4\text{Na}^+ + 4\text{e}^- \rightarrow \text{Mo}_{(\text{metallic})} + 2\text{Na}_2\text{S}$, a theoretical capacity of 670 mAh g⁻¹), leading to great electrochemical performance [13,14]. However, MoS₂ has an intrinsically low electronic conductivity, lowering the efficiency of (dis) charging SIB cells [15,16]. In addition, long channels of 2D MoS₂ interlayers are the bottleneck to Na⁺ diffusion, degrading SIB performance toward Na⁺ storage [17,18]. Furthermore, the dissolution of sulfur atoms contributes to a large loss in the overall mass after the conversion reactions, which is detrimental to achieving excellent battery performance. Therefore, we need to find a strategy to overcome the problems of MoS₂ mentioned above [19–21].

In this work, we successfully fabricated interlayer-enlarged MoS₂ nanoflakes, which were doubly covered with carbon nanofibers (CNFs), and reduced graphene oxide (rGO) (MoS₂@CNFs@rGO). The MoS₂ nanoflakes were first confined in the CNFs by thermolysis, subsequently encapsulated by the rGO via electrostatic interaction and reduction processes. The interlayers of MoS₂ nanoflakes in the CNFs were expanded during the thermolysis at 800 °C under the H₂ atmosphere. Moreover, the synergy of CNFs and rGO not only increase the electronic conductivity of the composite but also prevent the loss of S, enabling the SIB cells to be operated reversibly with a high capacity of 345.8 mA g⁻¹ for 90 cycles at a high current density of 100 mA g⁻¹. With the support of experimental and analytical studies, the underlying reaction mechanism of MoS₂@CNFs@rGO was investigated and proposed.

2. Materials and Methods

2.1. Experimental

Firstly, the MoS₂@CNFs were synthesized by electrospinning and a thermolysis process [17]. For the electrospinning, a solution containing 15 wt % of ammonium tetrathiomolybdate ((NH₄)₂MoS₄, ATTM, Alfa Aesar, Ward Hill, MA, USA) and 15 wt % of poly(styrene-acrylonitrile, SAN, Mw = 1,300,000) dissolved in 10 mL of *N,N*-dimethylformamide (DMF, Sigma-Aldrich, Burlington, MA, USA), was prepared on the hot plate by stirring the solution at 70 °C for 12 h. The solution was electrospun by applying a high voltage of 15 kV using an electrospinning machine (NanoNC, Seoul, South Korea). After the electrospinning, the electrospun NFs were thermally treated under H₂/Ar (4/96, *v/v*) surroundings at 450 °C for 2 h and under a pure Ar (99.999%) atmosphere at 800 °C for 6 h, respectively [17,22]. These processes were performed to make the MoS₂@CNFs. For wrapping the entire surfaces of MoS₂@rGO with the rGO, the Ti-O-Ti-O atomic layers (sub-nm) were coated on the MoS₂@rGO by using atomic layer deposition (ALD); this forms hydroxyl groups (OH-) of the atomic layers on MoS₂@rGO for rGO wrapping [7,23]. Then, poly(allylamine hydrochloride, Mw = 900,000, Sigma-Aldrich) was utilized as a surface modifier to form an amine group (NH₂-) on the surface, inducing a positively charged surface, i.e., -NH³⁺-grafted MoS₂@CNFs, in an aqueous solution. The MoS₂@rGO was added to the PAH solution. After stirring for 2 h, the PAH-modified MoS₂@rGO was rinsed three times with distilled water and dried at 60 °C in a vacuum oven overnight. Lastly, the modified sample was encapsulated with rGO according to the method in the same manner of our previous works [7,24], resulting in MoS₂@CNFs@rGO.

2.2. Materials Characterization

Nova 230 (field-emission scanning electron microscope (FE-SEM), FEI, Hillsboro, OR, USA) was employed to obtain FE-SEM images. The crystal structure of MoS₂@CNFs@rGO was investigated by X-ray diffraction (XRD) patterns using D/Max-2500, with RIGAKU Corp. (Tokyo, Japan) with Cu K α ($\lambda = 1.54 \text{ \AA}$) between 10° and 80° at a scan rate of

$0.066^\circ \text{ s}^{-1}$. Both internal and external morphologies of $\text{MoS}_2\text{@CNFs@rGO}$ and the distribution of elements were analyzed by a high-resolution transmission electron microscope (HR-TEM) operating at 300 kV and a scanning TEM (STEM) using a Tecnai F30 S-Twin (FEI, Hillsboro, OR, USA) equipped with energy-dispersive X-ray spectroscopy (EDX). The chemical states of $\text{MoS}_2\text{@CNFs@rGO}$ were investigated by X-ray photoelectron spectroscopy (XPS, K-alpha, Thermo VG Scientific, Waltham, MA, USA). In addition, the dominant vibration modes in the $\text{MoS}_2\text{@CNFs@rGO}$ were investigated using Raman spectroscopy (ARAMIS, Horiba Jobin Yvon, Montpellier, France) with a 514 nm laser source.

2.3. Electrochemical Evaluation

All the electrodes were prepared by casting a slurry, including active materials (80%), a conducting agent (Super-P, Sigma-Aldrich, Burlington, MA, USA) (10%), and a polyvinylidene fluoride (PVDF, $M_w \sim 534,000$, Sigma-Aldrich, Burlington, MA, USA) binder (10%); the slurry was mixed together using an agate mortar and cast on a copper foil as a current collector. After casting, the electrode was dried in a vacuum oven for 12 h. The mass loading of the $\text{MoS}_2\text{@CNFs@rGO}$ was approximately $1.0 \pm 0.1 \text{ mg cm}^{-2}$. Half-cell (2032 type-coin cell) assembly was done in an Ar-filled glovebox (water content $< 0.1 \text{ ppm}$). Na metal was used as a counter electrode, and a Whatman glass microfilter was employed as a separator for SIB cell tests. The used SIB electrolyte was 1 M NaClO_4 in propylene carbonate (PC) with 5 wt % of FEC. The assembled coin cells for Na storage were cycled at a current density of 100–20,000 mA g^{-1} between 0.005 and 3.0 V using a battery tester (WBCS3000 device by WonATech, Seoul, South Korea).

3. Results

3.1. Materials Characterization

The synthetic procedures to prepare the MoS_2 nanoflakes confined in CNFs wrapped with the rGO net ($\text{MoS}_2\text{@CNFs@rGO}$) are schematically illustrated in Figure 1. The MoS_2 -nanoflake-embedded carbon nanofibers ($\text{MoS}_2\text{@CNFs}$) were prepared by thermal treatment using ammonium tetrathiomolybdate ($(\text{NH}_4)_2\text{MoS}_4$) and poly(styrene-acrylonitrile) (SAN) as precursors through the electrospinning method (Figure 1a). First, the $(\text{NH}_4)_2\text{MoS}_4$ was decomposed into MoS_2 at 450°C in the presence of reducing (H_2) gas [25,26]. Then, carbonization and crystallization steps for MoS_2 are performed through heat treatment at 800°C under an inert gas environment. The reactions that occur during the heat treatment process are as follows.

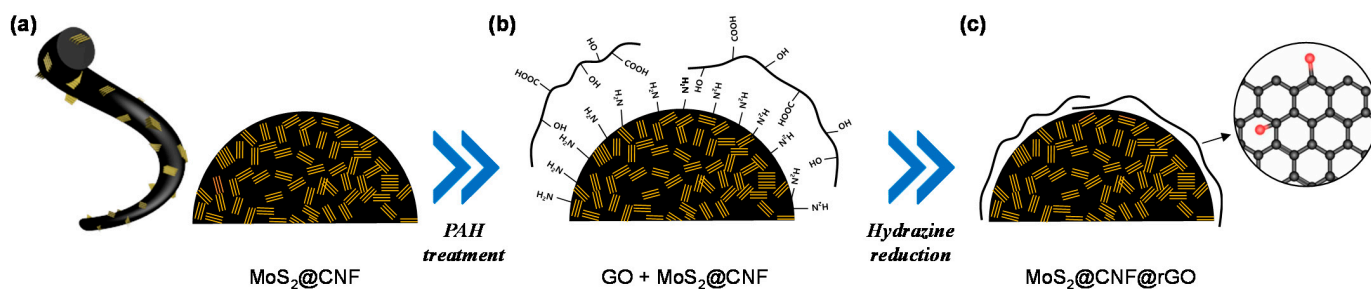
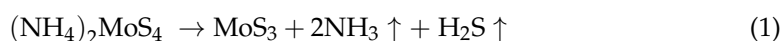


Figure 1. Schematic illustration for preparation of $\text{MoS}_2\text{@CNFs@rGO}$. (a) Fabrication of $\text{MoS}_2\text{@CNFs}$ synthesized by thermolysis after electrospinning. (b) Electrostatic interaction between PAH-modified $\text{MoS}_2\text{@CNFs}$ and GO. (c) The final product of rGO-wrapped $\text{MoS}_2\text{@CNFs}$ achieved after hydrazine reduction.

For rGO coating on the MoS₂@CNFs, the surface of MoS₂@CNFs was modified using poly(allylamine hydrochloride) (PAH) [7,23,24]. Firstly, the MoS₂@CNFs were dipped in PAH solution; the surface functional group changed from the hydroxy surface group to the amine group (-NH₂) (see the details in the Materials and Methods section). The PAH-modified MoS₂@CNFs have positively charged amine functional groups (NH₃⁺) exposed on the surface. On the other hand, the GO has functional groups of the carboxyl group (-COOH) and hydroxy group (-OH), attributed to the negative charge of GO in the aqueous solution. The GO flakes were quickly attracted to the surface of PAH-modified MoS₂@CNFs due to the electrostatic self-assembly (Figure 1b). Then, the GO was chemically reduced by hydrazine treatment, which rendered the strong chemical bond between the amine functional group and oxygen group with the ring-opening reaction. Finally, the GO changed to rGO, covering the entire surface of MoS₂@CNFs (Figure 1c).

The morphology of synthesized MoS₂@CNFs is shown in Figure 2a,b, demonstrating that the nanocomposite possessed one-dimensional (1D) NF networks, with the diameter of each fiber at about 200 nm and several micro-sized pores among the NFs. These pores facilitate electrolyte penetration to enhance electrochemical performance. The morphological change of MoS₂@CNFs@rGO was confirmed through SEM images (Figure 2c,d). It is confirmed that rGO flakes were covered on the NF surfaces while the 1D architecture of MoS₂@CNFs was maintained. To verify the internal structure and phase of the MoS₂@CNFs and MoS₂@CNFs@rGO, transmission electron microscopy (TEM) analysis was conducted. For the MoS₂@CNFs, few-layer MoS₂ flakes were uniformly distributed into CNFs (Figure 3a).

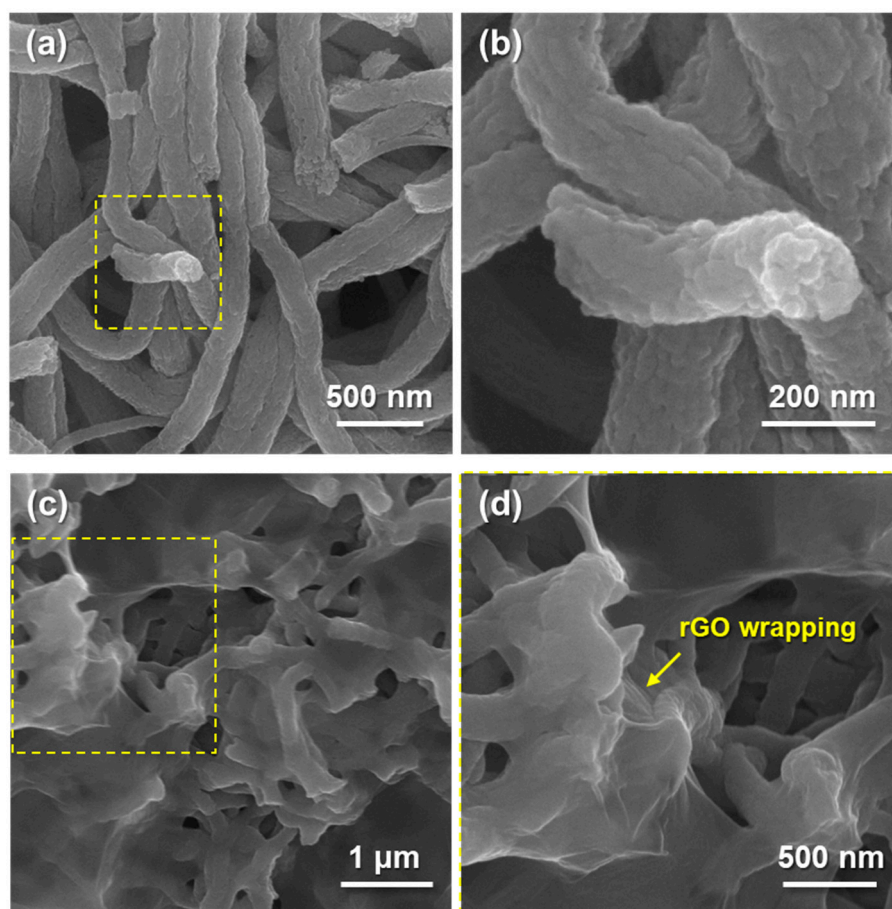


Figure 2. SEM images of (a) MoS₂@CNFs and (b) MoS₂@CNFs@rGO, HR-SEM images of (c) MoS₂@CNFs and (d) MoS₂@CNFs@rGO.

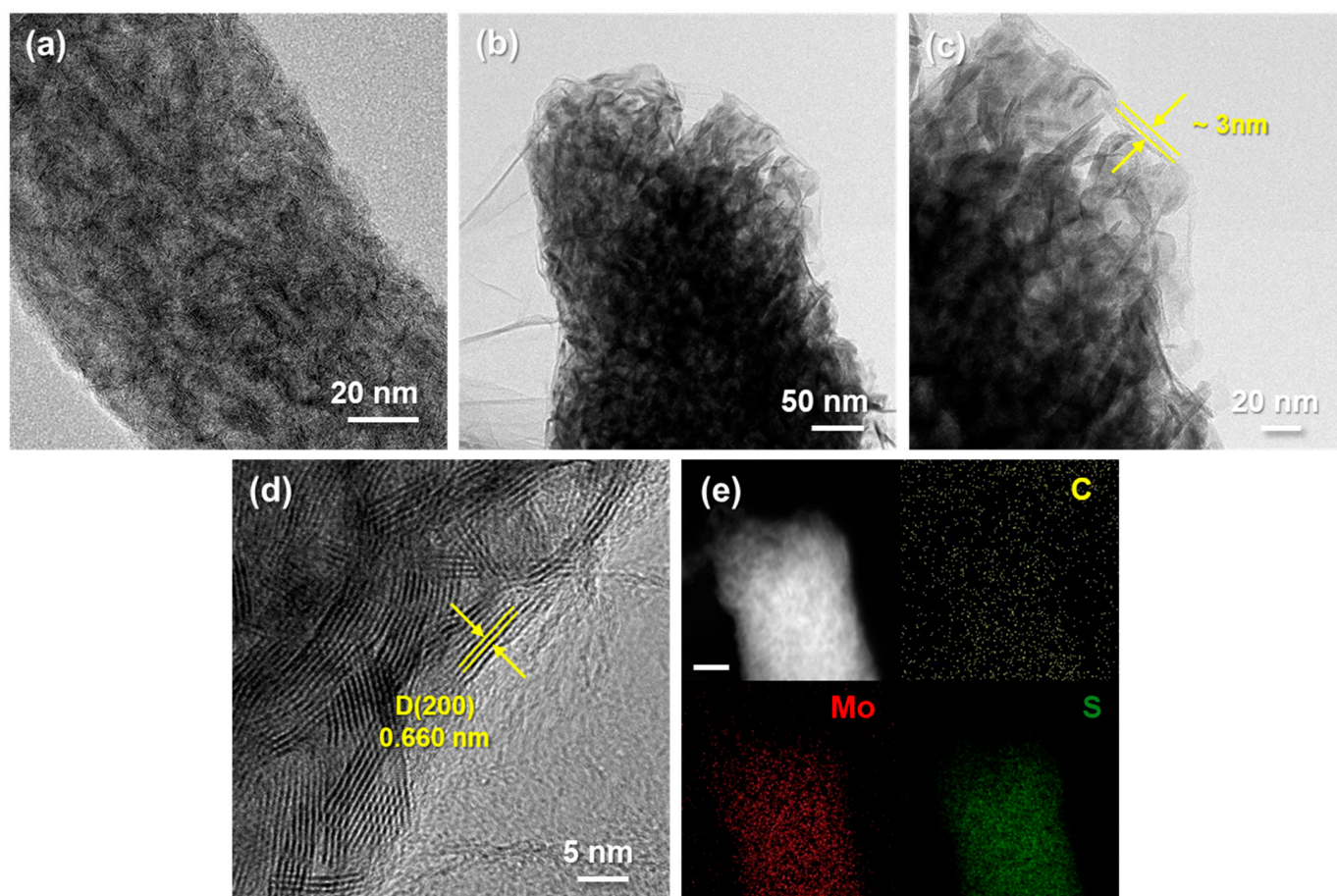


Figure 3. TEM images of (a) MoS₂@CNFs and (b) MoS₂@CNFs@rGO, (c,d) HR-TEM images of MoS₂@CNFs@rGO, (e) STEM image and elemental distribution of C, Mo, and S in the MoS₂@CNFs@rGO (scale bar: 20 nm).

After the graphene wrapping process, the rGO flakes substantially covered the MoS₂@CNFs without any aggregations. Individual NFs were wrapped by stacked rGO flakes with a thickness of approximately 3 nm (Figure 3b,c). We expected that the favorable influx of Na⁺ into MoS₂@CNFs would be possible through the thin rGO layer, and the electrically conductive rGO would enhance the electrical efficiency of the battery cell by facilitating the electron transport. Figure 3d shows a high-resolution TEM (HR-TEM) image of MoS₂@CNFs@rGO. The lattice fringe of the MoS₂ in the MoS₂@CNFs@rGO is approximately 0.660 nm, indicating that the multilayer MoS₂ nanoflakes had enlarged interlayer spacing compared to the general interlayer spacing (~0.615 nm) of multilayer MoS₂ [27,28]. The enlarged interlayers can be attributed to the CNFs suppressing the crystallization of MoS₂ during thermolysis. In addition, the wide interlayer distance might allow Na⁺ to diffuse rapidly, promoting Na⁺ flux in the whole electrode. The homogeneous distribution of elements—such as C (yellow), Mo (red), and S (green)—in the MoS₂@CNFs@rGO was investigated by energy-dispersive spectroscopy (EDS) mapping images from a scanning TEM (Figure 3e). The elements were well-distributed in the 1D NF composite, which can be supported by the qualitative data in Figure S1.

To further consider the crystal structure and phase information of the MoS₂@CNFs@rGO, Figure 4 exhibits the X-ray diffraction (XRD) patterns of MoS₂@CNFs and MoS₂@CNFs@rGO. At 14.2°, 33.3°, and 59.1°, the XRD peaks correspond to planes (002), (100), and (110) of the MoS₂ phase (JCPDS #37-1492), respectively [29]. Through the graphene wrapping process, no peak shifts were observed for MoS₂@CNFs@rGO. Furthermore, as a result of XPS analysis, the chemical states of Mo and C of MoS₂@CNFs@rGO showed insignificant change despite the chemical reduction reaction. (Figure S2). Figure 5 compares the Raman spectra of MoS₂@CNFs and MoS₂@CNFs and shows the vibrational modes, the fingerprint

of the chemical state of the MoS₂ phase. MoS₂@CNFs and MoS₂@CNFs@rGO represent two peaks at 379.1 and 402.7 cm⁻¹ due to in-plane E_{12g} and out-of-plane A_{1g} vibration modes [30]. Several studies exhibited that the relative intensity of these two peaks suggests the characteristics of MoS₂ crystals, given dimensions and edge profiles. Generally, the intensity of the A_{1g} mode is greater than that of the E_{12g} mode when the MoS₂ flakes have an edge-end structure. There is no difference between the E_{12g} and A_{1g} mode peaks for MoS₂@CNFs and MoS₂@CNFs@rGO, indicating that the MoS₂ nanoflakes in the CNFs maintain their structures without damage during the fabrication process. Furthermore, introducing the rGO layer increases the intensity of the D and G bands, which indicates the carbon structure (Figure 5b and Figure S3) [31,32]. The integrated area ratio of sp³ to sp² (Asp³/Asp²) has been proven to provide useful information concerning the nature of carbon [32]. The low ratio of Asp³/Asp² indicates the presence of a large amount of sp² carbon. The Asp³/Asp² were 1.31 for MoS₂@CNFs and 1.15 for MoS₂@CNFs@rGO, respectively. It means that the amount of sp²-type carbon increased after rGO wrapping and the reduced graphene oxide layers are well-introduced in the MoS₂@CNFs@rGO sample.

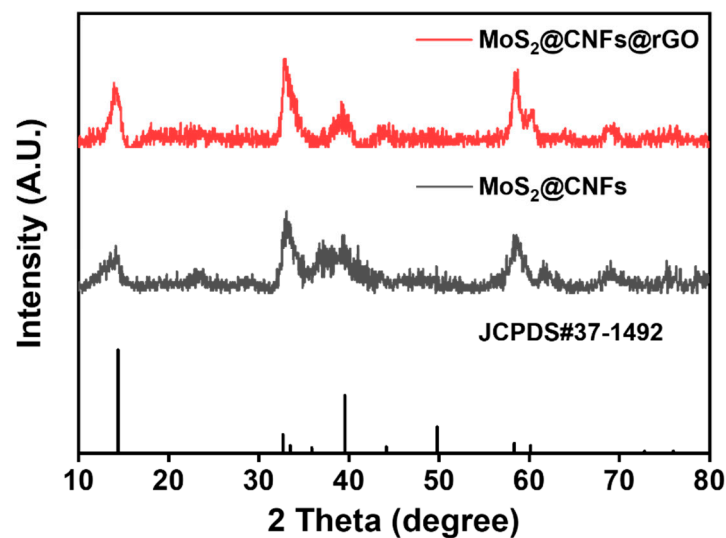


Figure 4. X-ray diffraction pattern of MoS₂@CNFs and MoS₂@CNFs@rGO.

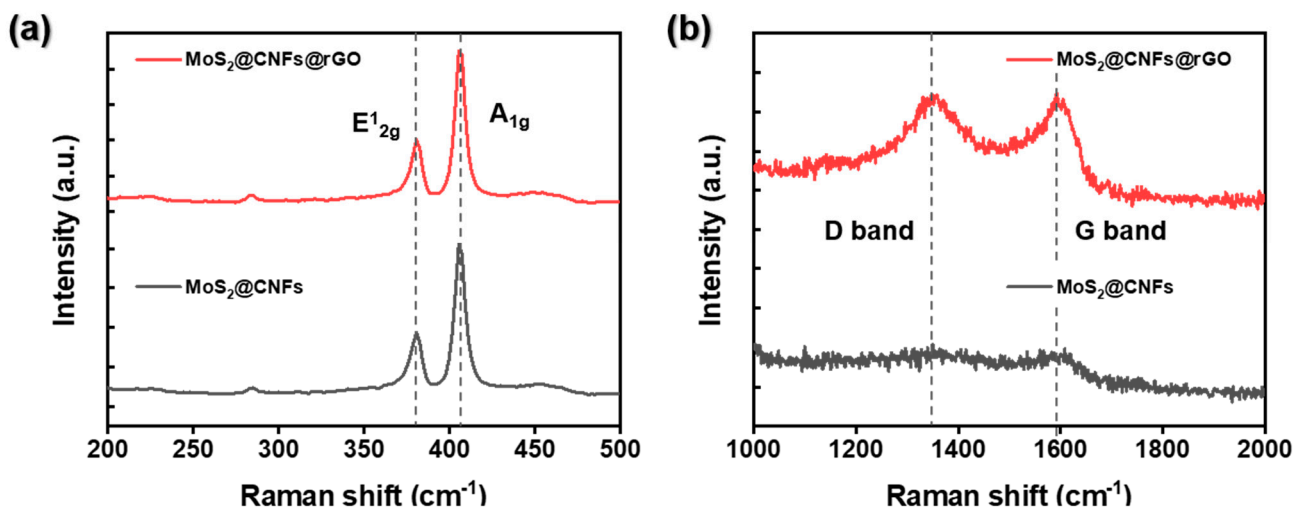


Figure 5. Results of Raman analyses of MoS₂@CNFs and MoS₂@CNFs@rGO with different ranges: (a) 200~500 cm⁻¹, (b) 1000~2000 cm⁻¹.

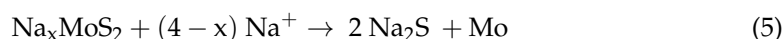
To quantitatively identify the contents of rGO in MoS₂@CNFs@rGO, element analysis (EA) was carried out (Table 1). The MoS₂@CNFs contain 23.6 wt % of carbon and about 29.8 wt % of sulfur from MoS₂. After graphene wrapping, the amount of carbon (C) increased to 34.3 wt %, indicating that the sulfur (S) content was relatively decreased. Assuming that the ratio of CNF/MoS₂ is maintained after graphene wrapping, it is confirmed that the content of rGO accounts for about 17.7 wt % in the MoS₂@CNFs@rGO. Since the 1D nanostructure of MoS₂@CNFs has a large surface area, a sufficient amount of rGO is required for the wrapping, even if it contains thin rGO layers. Therefore, the rGO should cover both the individual NFs and bundle of MoS₂@CNFs, increasing the electronic conductivity of the MoS₂@CNFs@rGO and preserving active materials, particularly S, during repetitive reactions [33,34].

Table 1. Contents of the carbon and sulfur components of MoS₂@CNFs and MoS₂@CNFs@rGO.

Samples	Carbon, C (wt %)	Sulfur, S (wt %)
MoS ₂ @CNFs	23.6	29.8
MoS ₂ @CNFs@ rGO	34.3	20.9

3.2. Electrochemical Measurement

In general, MoS₂ electrochemically reacts with Na⁺ based on insertion and conversion reactions [35]. To testify to these electrochemical behaviors in the MoS₂@CNFs@rGO, the galvanostatic charge-discharge curves for the MoS₂@CNFs@rGO were obtained in a voltage window between 0.005~3.0 V (vs. Na/Na⁺) at a current density of 100 mA g⁻¹ (Figure 6a). The initial discharge and charge capacities of MoS₂@CNFs@rGO are 1175 and 573 mAh g⁻¹, respectively, corresponding to a Coulombic efficiency (CE) of 48%. This capacity fading for the initial cycle is attributed to the generation of high irreversible capacitance stemming from the solid-electrolyte interphase (SEI) layers formed on the electrode with a large surface area. Nevertheless, in Figure S4, the initial CE of MoS₂@CNFs@rGO is higher than that of MoS₂@CNFs (44%). It appears that more SEI layers seem to form on the MoS₂@CNFs without the rGO coating layers while the rGO adequately stabilizes the SEI layers on the MoS₂@CNFs@rGO [36]. Moreover, rGO played a critical role in accelerating electron transport, which improved the initial CE of MoS₂@CNFs@rGO. It is confirmed that the MoS₂@CNFs@rGO has a voltage plateau at 1.4 V (vs. Na/Na⁺) and a slope thereafter. This can be explained by a reaction caused by the insertion of Na⁺ into MoS₂ (Equation (4)) and a subsequent conversion reaction (Equation (5)). Sodium polysulfide intermediate (Na₂S_x, where x = 2 to 5) generated by the conversion reaction are easily dissolved in liquid electrolyte and move to the Na anode (“polysulfide shuttling”), leading to capacity loss and adverse effects on battery operation. The overall reaction can be represented as [37–39]:



The voltage plateau generated at about 1.6 V in the charging process occurred due to the reduction of Na₂S to S. After the initial cycle, the SIB cell containing the MoS₂@CNFs@rGO electrode shows a highly reversible Na⁺ storage ability. We evaluated the long-term stability of MoS₂@CNFs@rGO, as shown in Figure 6b. The MoS₂@CNFs@rGO delivered a high discharge capacity of 345.8 mAh g⁻¹ at the 90th cycle with a CE of 99.8%. In addition, the rate capability of MoS₂@CNFs@rGO was tested at various current densities between 0.1~20 A g⁻¹ (Figure 6c). At lower rates, the MoS₂@CNFs@rGO exhibited similar capacity retention to that of MoS₂@CNFs. On the other hand, the rate capability of MoS₂@CNFs@rGO was gradually improved at higher rates (>0.5 A g⁻¹). Moreover, the MoS₂@CNFs@rGO outperformed the MoS₂@CNFs even at a super-fast rate of 20 A g⁻¹. This outstanding ability to store Na⁺ was also able to be used for Li⁺ storage (Figure S5).

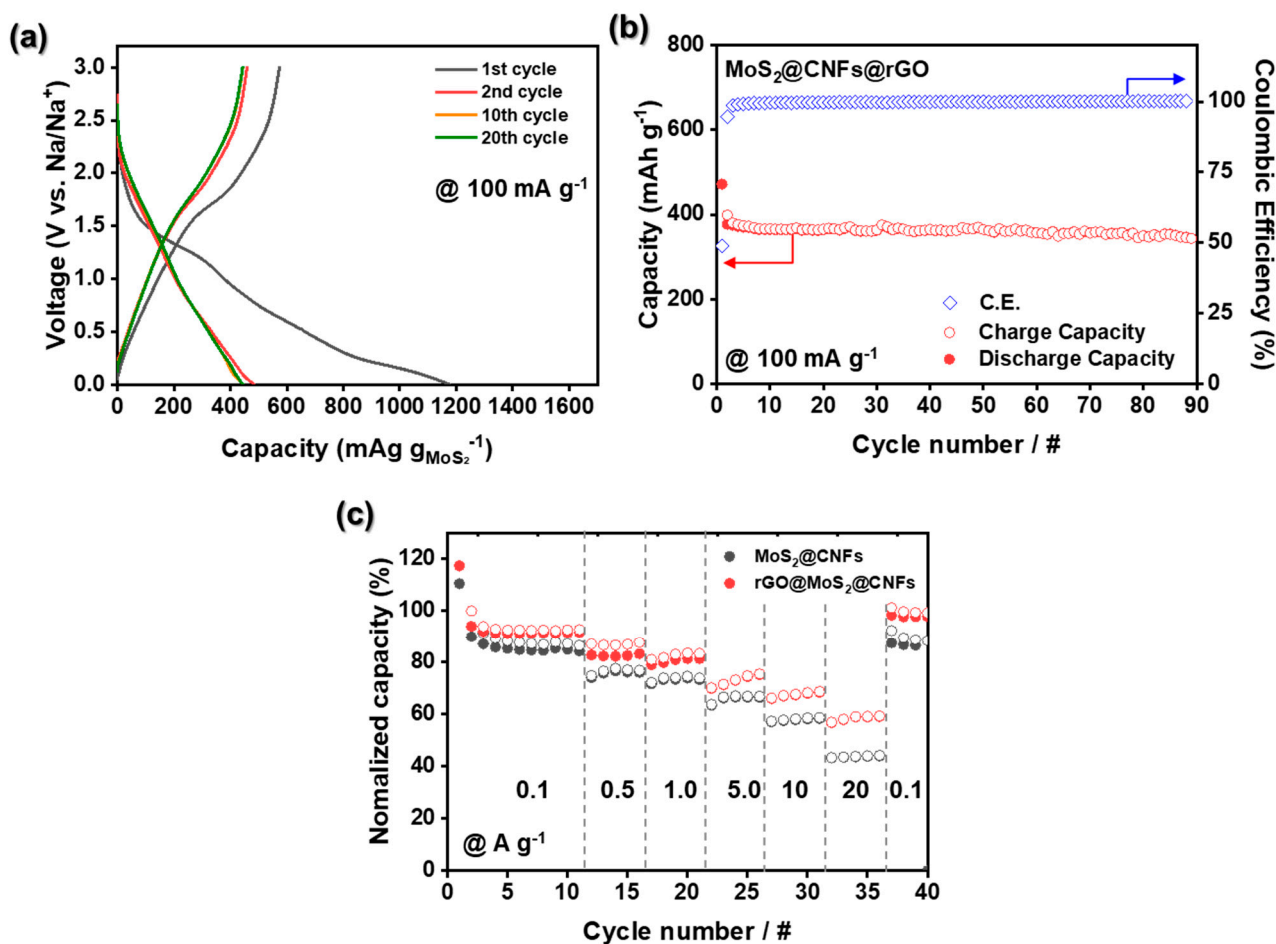


Figure 6. Electrochemical performances of MoS₂@CNFs@rGO. (a) Charge–discharge profile at 100 mA g⁻¹ between 0.005 V~3.0 V vs. Na/Na⁺. (b) Cycling performance at 100 mA g⁻¹. (c) Rate capability with different current densities (0.1~20 A g⁻¹).

All things taken together, we elucidated the reaction mechanism of MoS₂@CNFs@rGO, based on the following factors: (I) MoS₂ nanoflakes with enlarged interlayer spacing and short lateral distance between each flake are beneficial for storing Na⁺ in the CNFs. (II) The CNFs serve as a continuous passage for electrons and storage matrix for the active materials (Na⁺ and S). (III) The rGO is synergistically advantageous in terms of fast kinetics. Eventually, it turns out that the MoS₂@CNFs@rGO synthesized by our fabrication approach enables the SIB cells to show remarkable performance toward Na⁺ insertion and conversion reactions.

4. Conclusions

In summary, we report a straightforward approach to fabricate a composite consisting of MoS₂ nanoflakes confined in CNFs wrapped with a rGO net for SIB anodes. We effectively generated randomly distributed MoS₂ nanoflakes (a few layers) in the CNFs via thermolysis and wrapped the rGO onto the MoS₂@CNFs to enable the composite to be active for Na⁺ storage. The MoS₂ nanoflakes possessing short lateral and expanded interlayer distances would be favorable for reversible insertion/desertion of Na⁺. In addition, the strongly interconnected CNFs and rGO net promoted electron transfer through the whole electrode, rendering a high rate of capability and cyclability. Furthermore, the rGO would preclude the dissolution of S stemming from the conversion reactions at the outermost surfaces of the composite materials. The MoS₂@CNFs@rGO showed excellent cycle retention with a specific capacity of 345.8 mAh g⁻¹ at a current density of 100 mA g⁻¹ from

the initial cycle to the 90th cycle. We elucidated that in the MoS₂-based anodes undergoing conversion reactions, caging the active materials in the electronically conductive scaffold is critical for improving electrochemical battery performance.

Supplementary Materials: The following are available online at <https://www.mdpi.com/article/10.3390/nano11102691/s1>. Figure S1: EDS spectrum of rGO@MoS₂@CNFs, Figure S2: XPS analysis for MoS₂@CNFs@rGO and MoS₂@CNFs and for (a) C1s and (b) Mo 3d, Figure S3: Raman analysis for (a) MoS₂@CNFs@rGO and (b) MoS₂@CNFs with classified peaks (I, III: sp³ bonding, II, IV: sp² bonding), Figure S4: Charge–discharge curves of MoS₂@CNFs at a current density of 100 mA g^{−1}, Figure S5: Lithium-ion battery performance of MoS₂@CNFs@rGO.

Author Contributions: Conceptualization, S.-H.C. and J.-W.J.; methodology, S.-H.C., J.-H.K. and I.-G.K.; validation, S.-H.C., I.-G.K. and J.-H.P.; formal analysis and investigation, S.-H.C. and J.-W.J.; writing—original draft preparation, S.-H.C., J.-H.K. and J.-W.J.; writing—review and editing as well as supervision, J.-W.J., H.-S.K. and I.-D.K.; project administration and funding acquisition, J.-W.J. All authors have read and agreed to the published version of the manuscript.

Funding: This work was supported by the 2021 Research Fund of the University of Ulsan.

Institutional Review Board Statement: Not applicable.

Informed Consent Statement: Not applicable.

Data Availability Statement: Data are contained within the article.

Acknowledgments: This work was supported by the 2021 Research Fund of the University of Ulsan.

Conflicts of Interest: The authors declare no conflict of interest.

References

1. Senba, T. *Clean Disruption of Energy and Transportation*; Clean Planet Ventures: Silicon Valley, CA, USA, 2014; pp. 1–290.
2. Cano, Z.P.; Banham, D.; Ye, S.; Hintennach, A.; Lu, J.; Fowler, M.; Chen, Z. Batteries and fuel cells for emerging electric vehicle markets. *Nat. Energy* **2018**, *3*, 279–289. [[CrossRef](#)]
3. Tian, Y.; Zeng, G.; Rutt, A.; Shi, T.; Kim, H.; Wang, J.; Koettgen, J.; Sun, Y.; Ouyang, B.; Chen, T.; et al. Promises and Challenges of Next-Generation “Beyond Li-ion” Batteries for Electric Vehicles and Grid Decarbonization. *Chem. Rev.* **2021**, *121*, 1623–1669. [[CrossRef](#)]
4. Usiskin, R.; Lu, Y.; Popovic, J.; Law, M.; Balaya, P.; Hu, Y.-S.; Maier, J. Fundamentals, status and promise of sodium-based batteries. *Nat. Rev.* **2021**. [[CrossRef](#)]
5. Hwan, J.-Y.; Myung, S.-T.; Sun, Y.-K. Sodium-ion batteries: Present and future. *Chem. Soc. Rev.* **2017**, *46*, 3529–3614. [[CrossRef](#)] [[PubMed](#)]
6. Xiao, L.; Lu, H.; Fang, Y.; Sushko, M.L.; Cao, Y.; Ai, X.; Yang, H.; Liu, J. Low-Defect and Low-Porosity Hard Carbon with High Coulombic Efficiency and High Capacity for Practical Sodium Ion Battery Anode. *Adv. Energy Mater.* **2018**, *8*, 1703238. [[CrossRef](#)]
7. Yeo, Y.; Jung, J.-W.; Park, K.; Kim, I.-D. Graphene-Wrapped Anatase TiO₂ Nanofibers as High-Rate and Long-Cycle-Life Anode Material for Sodium Ion Batteries. *Sci. Rep.* **2015**, *5*, 13862. [[CrossRef](#)] [[PubMed](#)]
8. Wu, L.; Shao, H.; Yang, C.; Feng, X.; Han, L.; Zhou, Y.; Du, W.; Sun, X.; Xu, Z.; Zhang, X.; et al. SnS₂ Nanosheets with RGO Modification as High-Performance Anode Materials for Na-Ion and K-Ion Batteries. *Nanomaterials* **2021**, *11*, 1932. [[CrossRef](#)] [[PubMed](#)]
9. Hu, L.; Shang, C.; Akinoglu, E.M.; Wang, X.; Zhou, G. Cu₂Se Nanoparticles Encapsulated by Nitrogen-Doped Carbon Nanofibers for Efficient Sodium Storage. *Nanomaterials* **2020**, *10*, 302. [[CrossRef](#)] [[PubMed](#)]
10. Kim, D.-Y.; Kim, D.-H.; Kim, S.-H.; Lee, E.-K.; Park, S.-K.; Lee, J.-W.; Yun, Y.-S.; Choi, S.-Y.; Kang, J. Hard Carbon Anodes for Sodium-Ion Batteries. *Nanomaterials* **2021**, *9*, 793. [[CrossRef](#)]
11. Li, X.; Qi, S.-H.; Zhang, W.-C.; Feng, Y.-Z.; Ma, J.-M. Recent progress on FeS₂ as anodes for metal-ion batteries. *Rare Met.* **2020**, *39*, 1239–1255. [[CrossRef](#)]
12. Hu, R.; Fang, Y.; Liu, X.; Zhu, K.; Cao, D.; Yi, J.; Wang, G. Synthesis of SnS₂ Ultrathin Nanosheets as Anode Materials for Potassium Ion Batteries. *Chem. Res. Chin. Univ.* **2021**, *37*, 311–317. [[CrossRef](#)]
13. Yun, Q.; Li, L.; Hu, Z.; Lu, Q.; Chen, B.; Zhang, H. Layered Transition Metal Dichalcogenide-Based Nanomaterials for Electrochemical Energy Storage. *Adv. Mater.* **2019**, *32*, 1903826. [[CrossRef](#)]
14. Yun, Q.; Lu, Q.; Zhang, X.; Tan, C.; Zhang, H. Three-Dimensional Architectures Constructed from Transition-Metal Dichalcogenide Nanomaterials for Electrochemical Energy Storage and Conversion. *Angew. Chem. Int. Ed.* **2017**, *57*, 626–646. [[CrossRef](#)]
15. Wang, L.; Zhang, H.; Wang, Y.; Qian, C.; Dong, Q.; Deng, C.; Jiang, D.; Shu, M.; Pan, S.; Zhang, S. Unleashing ultra-fast sodium ion storage mechanisms in interface-engineered monolayer MoS₂/C interoverlapped superstructure with robust charge transfer networks. *J. Mater. Chem. A* **2020**, *8*, 15002–15011. [[CrossRef](#)]

16. Geng, X.; Jiao, Y.; Han, Y.; Mukhopadhyay, A.; Yang, L.; Zhu, H. Freestanding Metallic 1T MoS₂ with Dual Ion Diffusion Paths as High Rate Anode for Sodium-Ion Batteries. *Adv. Funct. Mater.* **2017**, *27*, 1702998. [[CrossRef](#)]
17. Jung, J.-W.; Ryu, W.-H.; Yu, S.; Kim, C.; Cho, S.-H.; Kim, I.-D. Dimensional Effects of MoS₂ Nanoplates Embedded in Carbon Nanofibers for Bifunctional Li and Na Insertion and Conversion Reactions. *ACS Appl. Mater. Interfaces* **2016**, *8*, 26758–26768. [[CrossRef](#)]
18. Li, Y.; Liang, Y.; Robles-Hernández, F.C.; Yoo, H.D. Enhancing sodium-ion battery performance with interlayer-expanded MoS₂-PEO nanocomposites. *Nano Energy* **2015**, *15*, 453–461. [[CrossRef](#)]
19. Ryu, W.-H.; Jung, J.-W.; Park, K.; Kim, S.-J.; Kim, I.-D. Vine-like MoS₂ anode materials self-assembled from 1-D nanofibers for high capacity sodium rechargeable batteries. *Nanoscale* **2014**, *6*, 10975–10981. [[CrossRef](#)]
20. Wang, L.; Yang, G.; Wang, J.; Peng, S.; Yan, W.; Ramakrishna, S. Controllable Design of MoS₂ Nanosheets Grown on Nitrogen-Doped Branched TiO₂/C Nanofibers: Toward Enhanced Sodium Storage Performance Induced by Pseudocapacitance Behavior. *Small* **2019**, *16*, 1904589. [[CrossRef](#)]
21. Huang, Y.; Wang, Z.; Guan, M.; Wu, F.; Chen, R. Toward Rapid-Charging Sodium-Ion Batteries using Hybrid-Phase Molybdenum Sulfide Selenide-Based Anodes. *Adv. Mater.* **2020**, *32*, 2003534. [[CrossRef](#)]
22. Kim, M.; Seok, H.; Selvam, N.C.S.; Cho, J.; Choi, G.H.; Nam, M.G.; Kang, S.; Kim, T.; Yoo, P.J. Kirkendall effect induced bifunctional hybrid electrocatalyst (Co₉S₈@MoS₂/N-doped hollow carbon) for high performance overall water splitting. *J. Power Source* **2021**, *493*, 229688. [[CrossRef](#)]
23. Zhou, W.; Zhu, J.; Cheng, C.; Liu, J.; Yang, H.; Cong, C.; Guan, C.; Jia, X.; Fan, H.J.; Yan, Q.; et al. A general strategy toward graphene@metal oxide core-shell nanostructures for high-performance lithium storage. *Energy Environ. Sci.* **2011**, *4*, 4954–4961. [[CrossRef](#)]
24. Cho, S.-H.; Jung, J.-W.; Kim, C.; Kim, I.-D. Rational Design of 1-D Co₃O₄ Nanofibers@Low content Graphene Composite Anode for High Performance Li-Ion Batteries. *Sci. Rep.* **2017**, *7*, 45105. [[CrossRef](#)] [[PubMed](#)]
25. Brio, J.L.; Ilija, M.; Hernández, P. Thermal and reductive decomposition of ammonium thiomolybdates. *Thermochim. Acta* **1995**, *256*, 325–338. [[CrossRef](#)]
26. Müller, A.; Prasad, T.P.; Menge, R. Thermal decomposition of (NH₄)₂MoS₄ and (NH₄)₂WS₄ heat of formation of (NH₄)₂MoS₄. *Z. Für Anorg. Und Allg. Chem.* **1972**, *391*, 107–112. [[CrossRef](#)]
27. Wu, C.; Song, H.; Tang, C.; Du, A.; Yu, C.; Huang, Z.; Wu, M.; Zhang, H. Ultralarge interlayer distance and C,N-codoping enable superior sodium storage capabilities of MoS₂ nanoions. *Chem. Eng. J.* **2019**, *378*, 122249. [[CrossRef](#)]
28. Sahu, T.S.; Mitra, S. Exfoliated MoS₂ Sheets and Reduced Graphene Oxide-An Excellent and Fast Anode for Sodium-ion Battery. *Sci. Rep.* **2015**, *5*, 12571. [[CrossRef](#)] [[PubMed](#)]
29. Yang, L.; Cui, X.; Zhang, J.; Wang, K.; Shen, M.; Zeng, S.; Dayeh, S.A.; Feng, L.; Xiang, B. Lattice strain effects on the optical properties of MoS₂ nanosheets. *Sci. Rep.* **2014**, *4*, 5649. [[CrossRef](#)]
30. Scheuschner, N.; Gillen, R.; Staiger, M.; Maultzsch, J. Interlayer resonant Raman modes in few-layer MoS₂. *Phys. Rev. B* **2015**, *91*, 235409. [[CrossRef](#)]
31. Wu, J.-B.; Lin, M.-L.; Cong, X.; Liu, H.-N.; Tan, P.-H. Raman spectroscopy of graphene-based materials and its applications in related devices. *Chem. Soc. Rev.* **2018**, *47*, 1822–1873. [[CrossRef](#)]
32. Abdelaal, M.M.; Hung, T.-C.; Mohamed, S.G.; Yang, C.-C.; Huang, H.-P.; Hung, T.-F. A Comparative Study of the Influence of Nitrogen Content and Structural Characteristics of NiS/Nitrogen-Doped Carbon Nanocomposites on Capacitive Performances in Alkaline Medium. *Nanomaterials* **2021**, *11*, 1867. [[CrossRef](#)] [[PubMed](#)]
33. Huang, Y.; Zhang, L.; Lu, H.; Lai, F.; Miao, Y.-E.; Liu, T. A highly flexible and conductive graphene-wrapped carbon nanofiber membrane for high-performance electrocatalytic application. *Inorg. Chem. Front.* **2016**, *3*, 969–976. [[CrossRef](#)]
34. Cai, J.; Reinhart, B.; Eng, P.; Liu, Y.; Sun, C.-J.; Zhou, H.; Ren, Y.; Meng, X. Nitrogen-doped graphene-wrapped Cu₂S as a superior anode in sodium-ion batteries. *Carbon* **2020**, *170*, 430–438. [[CrossRef](#)]
35. Wang, R.; Wang, S.; Zhang, Y.; Jin, D.; Tao, X.; Zhang, L. Sodium storage in a promising MoS₂-carbon anode: Elucidating structural and interfacial transitions in the intercalation process and conversion reactions. *Nanoscale* **2018**, *10*, 11165–11175. [[CrossRef](#)]
36. Prosini, P.P.; Carewska, M.; Cento, C.; Tarquini, G.; Maroni, F.; Birrozzi, A.; Nobili, F. Tin-Decorated Reduced Graphene Oxide and NaLi_{0.2}Ni_{0.25}Mn_{0.75}O₈ as Electrode Materials for Sodium-Ion Batteries. *Materials* **2019**, *12*, 1074. [[CrossRef](#)]
37. Lei, T.; Chen, W.; Lv, W.; Huang, J.; Zhu, J.; Chu, J.; Yan, C.; Wu, C.; Yan, Y.; He, W.; et al. Inhibiting Polysulfide Shuttling with a Graphene Composite Separator for Highly Robust Lithium-Sulfur Batteries. *Joule* **2018**, *2*, 2091–2104. [[CrossRef](#)]
38. Xu, X.; Zhou, D.; Qin, X.; Lin, K.; Kang, F.; Li, B.; Shanmukaraj, D.; Rojo, T.; Armand, M.; Wang, G. A room-temperature sodium-sulfur battery with high capacity and stable cycling performance. *Nat. Commun.* **2018**, *9*, 3870. [[CrossRef](#)] [[PubMed](#)]
39. Mosa, J.; Garcia-Garcia, F.J.; González-Elipe, A.R.; Aparicio, M. New Insights on the Conversion Reaction Mechanism in Metal Oxide Electrodes for Sodium-Ion Batteries. *Nanomaterials* **2021**, *11*, 966. [[CrossRef](#)] [[PubMed](#)]